Neurobiology of Disease 200 (2024) 106613

Contents lists available at ScienceDirect

Neurobiology of Disease

journal homepage: www.elsevier.com/locate/ynbdi

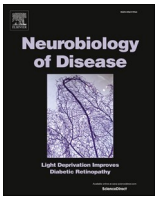

Whole-brain model replicates sleep-like slow-wave dynamics generated by stroke lesions

Sebastian Idesis [a,*], Gustavo Patow [a,b], Michele Allegra [c,d], Jakub Vohryzek [a,j], Yonatan Sanz Perl [a,g,h,i], Maria V. Sanchez-Vives [k,l], Marcello Massimini [m,n], Maurizio Corbetta [c,e,f], Gustavo Deco [a]

[a] Center for Brain and Cognition (CBC), Department of Information Technologies and Communications (DTIC), Pompeu Fabra University, Edifici Mercè Rodoreda, Carrer Trias i Fargas 25-27, 08005 Barcelona, Catalonia, Spain
[b] ViRVIG, University of Girona, Girona, Spain
[c] Padova Neuroscience Center (PNC), University of Padova, via Orus 2/B, 35129 Padova, Italy
[d] Department of Physics and Astronomy "G. Galilei", University of Padova, via Marzolo 8, 35131 Padova, Italy
[e] Department of Neuroscience University of Padova, via Giustiniani 5, 35128 Padova, Italy
[f] Venetian Institute of Molecular Medicine (VIMM), via Orus 2/B, 35129 Padova, Italy
[g] Universidad de San Andrés, Buenos Aires, Argentina
[h] National Scientific and Technical Research Council, Buenos Aires, Argentina
[i] Institut du Cerveau et de la Moelle épinière, ICM, Paris, France
[j] Centre for Eudaimonia and Human Flourishing, Linacre College, University of Oxford, UK
[k] Institut d'Investigacions Biomèdiques August Pi i Sunyer (IDIBAPS), Rosellón, 149, 08036 Barcelona, Spain
[l] Institució Catalana de Recerca i Estudis Avançats (ICREA), Passeig de Lluís Companys, 23, 08010 Barcelona, Spain
[m] Department of Biomedical and Clinical Sciences, University of Milan, Milan 20157, Italy
[n] IRCCS, Fondazione Don Carlo Gnocchi Onlus, Milan 20148, Italy

ARTICLE INFO

Keywords:
Whole-brain models
Predictive
Stroke
(f)MRI
Sleep-like slow waves

ABSTRACT

Focal brain injuries, such as stroke, cause local structural damage as well as alteration of neuronal activity in distant brain regions. Experimental evidence suggests that one of these changes is the appearance of sleep-like slow waves in the otherwise awake individual. This pattern is prominent in areas surrounding the damaged region and can extend to connected brain regions in a way consistent with the individual's specific long-range connectivity patterns. In this paper we present a generative whole-brain model based on (f)MRI data that, in combination with the disconnection mask associated with a given patient, explains the effects of the sleep-like slow waves originated in the vicinity of the lesion area on the distant brain activity. Our model reveals new aspects of their interaction, being able to reproduce functional connectivity patterns of stroke patients and offering a detailed, causal understanding of how stroke-related effects, in particular slow waves, spread throughout the brain. The presented findings demonstrate that the model effectively captures the links between stroke occurrences, sleep-like slow waves, and their subsequent spread across the human brain.

1. Introduction

The functional consequences resulting from a focal brain lesion, e.g., an ischemic stroke, can be attributed both to direct structural damage and to indirect changes in the functioning of nearby and interconnected brain regions (Corbetta et al., 2015). Moreover, it is believed that focal cortical injuries have the potential to disrupt neuronal activity on a broader scale, affecting large-scale networks that extend beyond the specific area of neuronal loss (Falcon et al., 2016). This phenomenon of functional alterations occurring in brain structures not directly affected by structural damage is referred to as "diaschisis" (Carrera and Tononi, 2014; Die Lokalisation im Grosshirn und der Abbau der Funktion durch Kortikale Herde, 1914).

Evidence from electrophysiological studies conducted in animal models and from non-invasive clinical recordings of individuals with stroke and traumatic brain injuries suggests a noticeable slowing of

* Corresponding author.
E-mail address: sebastian.idesis@gmail.com (S. Idesis).

https://doi.org/10.1016/j.nbd.2024.106613
Received 26 March 2024; Received in revised form 17 June 2024; Accepted 22 July 2024
Available online 28 July 2024

electroencephalographic (EEG) and magnetoencephalographic (MEG) rhythms, particularly in regions on the same side as the brain lesion (Butz et al., 2004; Nuwer et al., 1987). In addition, recent work using direct cortical perturbations with transcranial magnetic stimulation (TMS) has proposed the occurrence of slow EEG responses in the perilesional area, a phenomenon that is associated with disruptions in local information processing (Sarasso et al., 2020). In parallel, intracranial recordings showed that in patients undergoing radiofrequency thermocoagulation, the activity in areas adjacent to the lesion during wakefulness exhibited slow waves that closely resembled those observed during baseline non-rapid eye movement (NREM) sleep in the same individuals (Russo et al., 2021). Notably, these sleep-like slow waves were particularly prominent in the perilesional areas but could also spread through a network of connected regions, as predicted by the individual's patterns of long-range effective connectivity (Sarasso et al., 2020). This distant effect was even empirically observed in several contacts located up to 6 cm away from the lesion's centroid, which displayed a notable increase in delta power (Russo et al., 2021).

In a recent review, Massimini and colleagues (Massimini et al., 2024) suggest the intriguing possibility that the intrusion of low-frequency neuronal activity into anatomically unaffected cortical tissue represents a significant element contributing to functional network disruption following brain injuries (Russo et al., 2021). As such, it was proposed that the generation of focal sleep-like slow waves and their propagation across long distances within the awake brain may constitute a crucial electrophysiological aspect of diaschisis and, more broadly, a key factor in comprehending the functional consequences of focal and multi-focal injuries (Russo et al., 2021).

The concept of a localized slowing of wake EEG activity surrounding focal lesions has roots in early recordings of acute stroke patients (Nuwer et al., 1987). However, as the use of electrophysiology in stroke research gave way to structural and metabolic imaging techniques, our understanding of EEG slow rhythms in humans following strokes suffered from considerable delays, as reported recently in a review from Massimini and colleagues (Massimini et al., 2024). While compelling evidence has shown that slow waves appeared as highly synchronic discharges, interspersed with silent periods, or off-periods, that interrupt processing and causal interactions (Camassa et al., 2022), the relationship between localized slow waves occurring after focal brain injuries and the electrophysiology of natural sleep slow waves remains unclear (Clarkson et al., 2010; Nita et al., 2006). In this line, previous studies have looked into the relation of slow waves during wakefulness with behavior (Andrillon et al., 2021) and have used novel methods to track this sleep-like intrusions in fMRI data (Poudel et al., 2021). On the contrary, in a global methodology, whole-brain human models integrate structural neuroanatomical data (utilizing diffusion tensor imaging) and brain activity data (comprising fMRI, EEG, and MEG). Anatomical connectivity, mostly provided through MRI, is represented by the density of axonal fibers according to a specific parcellation scheme. In these models, global dynamics emerge from the interactions of local node dynamics, coupled through the underlying structural connectivity matrix.

Inspired by the discussion presented in a recent article (Massimini et al., 2024) in this study, we aim to implement a generative model able to predict the effects of lesions on connectivity by using (f)MRI data of healthy controls and stroke patients. We employed an approximation of local dynamics, that is, a biophysically realistic mean-field model for spiking neurons (Deco et al., 2009; Deco and Jirsa, 2012). Although in this paper we provide a self-contained overview, the detailed mathematical formulation of this biophysical, realistic and dynamical mean-field model can be found elsewhere (Deco et al., 2014b). As a first step, for this predictive model, the whole-brain model will be calibrated using the fMRI functional connectivity (FC) matrices of participants from the healthy control group as performed in a previous study (Idesis et al., 2024a). Subsequently, to individually generate the FC matrix for each stroke patient, their real disconnection patterns were considered, simulating a damage to the healthy control model. Finally, we induce sleep-like slow waves in the affected local regions by introducing a specially tailored low frequency oscillation (Deco et al., 2014a). Simulations from our model indicate that perilesional sleep-like slow waves, and their spread across the human brain, can contribute to explaining FC alterations observed in stroke patients. Future studies may test our model's prediction with EEG recordings in stroke patients.

Leveraging a large-scale (f)MRI database of healthy controls and stroke patients, in this study we aim to understand the possible local and distal effects of slow-wave activity in stroke patients' resting state connectivity, by implementing a generative model accounting for the emergence of slow waves in the perilesional area. Our results show that the proposed model effectively captures the relationships between lesion areas, sleep-like slow waves, and their spread across the human brain. In summary, our generative whole-brain framework provides a detailed, causally mechanistic explanation of the relationship between stroke damage and its propagation. These results are essential for developing strategies for diagnosis, prediction, and, most importantly, stimulation-based recovery.

2. Methods

2.1. Overview

We used the Washington University Stroke Cohort dataset consisting of three cohorts of stroke-lesioned patients: after 1 or 2 weeks of the incident, 3 months and 1 year after onset, followed by a carefully tailored preprocessing (see below). Then, each lesion was manually segmented on the scans and verified by two board-certified neurologists. From this, the lesion volume was obtained from a voxel-wise analysis of the structural lesions. Using these volumes, a Lesion Disconnection Mask (see "Lesion disconnection masks" section) was built for each patient by counting the number of streamlines spared by the lesion. Then, at the simulation stage, a Dynamic Mean Field (DMF) using the Feedback Inhibition Control Mechanism was simulated and fed into a BOLD computation. This model was first used in the context of a Generative Effective Connectivity loop, which used the model to find the effective connectivity linking every pair of regions. Once this structural connectivity replacement was found, two different models were explored: First, a non-slow-wave (***non-SWS***) predictive model, that simply used the DMF model to assess the performance of the lesioned brains and compared it to the same model incorporating the slow-wave sleep (***SWS***) signal at the peri-lesion area. Finally, surrogates were computed and used to assess the validity of the proposed approach.

Code and sample data are available at: https://github.com/SebastianIdesis/SWS_Model

2.2. Subjects

We used the Washington University Stroke Cohort dataset (Corbetta et al., 2015). Despite being a longitudinal dataset, this study focuses on patients experiencing their first-time, single lesion stroke, predominantly ischemic (83%) with a minority being hemorrhagic (17%). Our analysis solely concentrated on data collected at the initial time point, within 1–2 weeks post stroke (mean = 13.4 days, SD = 4.8 days). Additionally, we examined a control group matched for age, consisting of 27 healthy individuals, who were assessed twice, three months apart. From this cohort, we selected 96 stroke patients (M = 57%, F = 43%) and 27 healthy subjects (M = 59%, F = 41%) as performed in previous literature (Idesis et al., 2022b, 2023, 2024a). Details of patients' demographic information and lesion location could be found in the original manuscript (Corbetta et al., 2015). The number of patients and controls in the study was fixed based on availability due to similar recording length and high data quality. Patients with low data quality were discarded as in previous publications (Idesis et al., 2022b, 2023, 2024a).

Stroke patients were prospectively recruited from the stroke service at Barnes-Jewish Hospital (BJH), with the help of the Washington University Cognitive Rehabilitation Research Group (CRRG). The complete data collection protocol is described in full detail in a previous publication (Corbetta et al., 2015). Healthy controls were selected based on the same inclusion/exclusion criteria as described in the original study (Corbetta et al., 2015). This group typically constituted of spouses or first-degree relatives of the patients, age- and education-matched to the stroke sample. Patients were characterized with a robust neuroimaging battery for structural and functional features, and an extensive (~2 h) neuropsychological battery.

2.3. Neuroimaging acquisition and preprocessing

As mentioned, we use data from the Washington University Stroke Cohort, extensively described in previous articles (Corbetta et al., 2015; Idesis et al., 2022a, 2022b; Siegel et al., 2016, 2018). A brief description of the data acquisition and preprocessing follows, while a complete description of it is explained in detail in a previous publication (Griffis et al., 2019).

Neuroimaging data were collected using a Siemens 3 T Tim-Trio scanner with a 12-channel head coil. It was obtained sagittal T1-weighted MP-RAGE (TR = 1950 msec; TE = 2.26 msec, flip angle = 90 degrees; voxel dimensions = 1.0 × 1.0 × 1.0 mm), and gradient echo EPI (TR = 2000 msec; TE = 2 msec; 32 contiguous slices; 4 × 4 mm in-plane resolution) resting-state functional MRI scans from each subject. Participants were instructed to fixate on a small centrally located white fixation cross that was presented against a black background on a screen at the back of the magnet bore. Between six and eight resting-state scans (128 volumes each) were obtained from each participant (~30 min total) giving a total of 768–1024 time points for each participant. The vast majority of subjects had 7 scans (896 points).

Resting-state fMRI preprocessing included (i) regression of head motion, signal from ventricles and CSF, signal from white matter, global signal (ii) temporal filtering retaining frequencies in 0.009–0.08 Hz band: and (iii) frame censoring, FD = 0.5 mm. Finally, the resulting time series were projected on the cortical and subcortical surface of each subject divided into 234 ROIs (200 cortical plus 34 subcortical).

These areas are taken from the multi-resolution functional connectivity-based cortical parcellations developed by Schaefer and colleagues (Schaefer et al., 2018), including additional subcortical and cerebellar parcels from the Automated Anatomical Labeling (AAL) atlas (Tzourio-Mazoyer et al., 2002) and a brainstem parcel from the Harvard-Oxford Subcortical atlas (https://fsl.fmrib.ox.ac.uk/fsl/fslwiki/Atlases).

2.4. Stroke deficit assessment

- Lesion volume and severity

Lesion volume was calculated based on the topography of stroke using a voxel-wise analysis of structural lesions. Each lesion was manually segmented on structural MRI scans and checked by two board-certified neurologists. The location (cortico-subcortical, subcortical, white-matter) of each individual lesion was assigned with an unsupervised K-means clustering algorithm on the percentage of total cortical/subcortical gray and white matter masks overlay. The overlap of each lesion group with gray matter, white matter and subcortical nuclei is explained in detail in a previous publication (Corbetta et al., 2015). In addition to the anatomical lesion volume, the patients' clinical severity was assessed through the National Institutes of Health Stroke Scale (NIHSS) (Brott et al., 1989) that includes 15 subtests addressing: level of consciousness (LOC), gaze and visual field deficits, facial palsy, upper and lower motor deficits, limb ataxia, sensory impairment, inattention, dysarthria and language deficits. The total NIHSS score was used as an averaged measure of the clinical severity for each patient. The lesion volume relation with the NIHSS was assessed, showing a significant association ($p < .01$) (Idesis et al., 2023). The metric of total disconnection tracks was described in detail in previous literature (Griffis et al., 2019).

- ***Lesion disconnection masks***

The Lesion Quantification Toolkit (Griffis et al., 2021) produces a comprehensive set of atlas-derived lesion measures that include measures of gray matter damage, white matter disconnection, and alterations of higher-order brain network topology. Importantly, the measures produced by the toolkit are based on population-scale (N = 842) atlases of gray matter parcel boundaries and white matter connection trajectories that were constructed from high-quality resting-state functional MRI and diffusion MRI data using state-of-the-art methods. Healthy controls group-averaged structural connectivity (SC) consisted in anatomical connections between the regions of interest and was calculated based on the afore-mentioned population-scale atlases.

To compute an individual structural connectivity for each patient, we did not directly measure disconnection (e.g., by using diffusion imaging), but used a model-based approach where the structural connectivity loss is inferred based on lesion location. Taking advantage of the Lesion Quantification Toolkit (LQT) (Griffis et al., 2021), the structural disconnection (SDC) mask consist of an adjacency matrix of spared connections where each cell (i,j) quantifies the percentage of streamlines, among those connecting the pair of regions (i,j), that are spared by the lesion, when the latter is superimposed on an the atlas-based structural connectome. The multiplication of each SDC mask (model-based, derived from the LQT) with the group-averaged SC (Griffis et al., 2021) provides an atlas-based estimate of structural connectivity links in individual patients. The SDC masks were computed embedding the lesion in the healthy structural connectivity atlas. Therefore, the measures of structural disconnection were indirectly derived.

Since many stroke lesions occur predominantly in the white matter, or include both a gray and white matter component, the SDC mask should provide an accurate description of the damage to the connectome. Thus, we computed the total amount of disconnection (Griffis et al., 2019) as a metric of anatomical impairment to assess the validity of the model.

2.5. Whole-brain dynamic mean field model

The Dynamic Mean Field (DMF) model previously introduced (Deco et al., 2014b) is a mean-field approximation that uses a set of coupled stochastic differential equations to model the dynamics of the activity at one or more interacting brain regions. The key idea behind mean-field approximations is to reduce a high-dimensional system of randomly interacting elements (i.e., neurons) to a system of elements treated as independent entities. In this approach, the average activity of a homogeneous population of neurons is represented by the activity of a single unit of this class. In the DMF model, each brain region is modelled as two coupled neuronal masses — one excitatory and one inhibitory — and considers excitatory and inhibitory synaptic currents mediated by NMDA, AMPA (excitatory) and GABA (inhibitory) receptors. Different brain regions (usually defined by a given brain parcellation) are coupled via their excitatory populations exclusively, according to the structural connectivity matrix:

$$I_i^{(E)} = I_i^{ext} + W_E I_0 + W_+ J_{NMDA} S_i^{(E)} + J_{NMDA} \sum_j C_{ij} S_j^{(E)} - J_i S_i^{(I)}, \quad (1)$$

$$I_i^{(I)} = W_I I_0 + J_{NMDA} S_i^{(E)} - S_i^{(I)}, \quad (2)$$

$$r_i^{(E)} = H^{(E)}\left(I_i^{(E)}\right) = \frac{a_E I_i^{(E)} - b_e}{1 - exp\left(-d_E\left(a_E I_i^{(E)} - b_e\right)\right)}, \quad (3)$$

$$r_i^{(I)} = H^{(I)}\left(I_i^{(I)}\right) = \frac{a_I I_i^{(I)} - b_I}{1 - exp\left(-d_I\left(a_I I_i^{(I)} - b_I\right)\right)}, \quad (4)$$

$$\frac{dS_i^{(E)}(t)}{dt} = \frac{S_i^{(E)}}{\tau_E} + \left(1 - S_i^{(E)}\right)\gamma r_i^{(E)} + \sigma v_i(t), \quad (5)$$

$$\frac{dS_i^{(I)}(t)}{dt} = \frac{S_i^{(I)}}{\tau_I} + r_i^{(I)} + \sigma v_i(t), \quad (6)$$

This model also includes a self-regulating mechanism from the inhibitory population on the excitatory one to keep regional natural oscillating frequencies at around 3 Hz, called the Feedback Inhibition Control Mechanism (Deco et al., 2014b; Herzog et al., 2022). In this study, we base our implementation on a version of the model presented in a previous article by Herzog and colleagues (Herzog et al., 2022). It is important to clarify that the inspection of low-dimensional features in a stroke population has been reported in the previous literature (Idesis et al., 2023; Talozzi et al., 2023).

2.6. Simulated BOLD signal

We used the generalized hemodynamic model of Stephan and colleagues (Stephan et al., 2007) to simulate the regional BOLD signals in the model. Global regression was performed in both empirical and simulated data. We calculate the BOLD signal in each brain area n from the simulated BEI model firing rate of the excitatory pools $r_n^{(E)}$, from Eq. 3. In this hemodynamic model, an increase in the firing rate causes an increase in a vasodilatory signal, s_n, that is subject to auto-regulatory feedback. Blood inflow f_n responds in proportion to this signal, inducing changes in blood volume v_n and deoxyhemoglobin content q_n. The set of equations describing the hemodynamic model coupling these biophysical variables are:

$$\frac{ds_i(t)}{dt} = 0.5z_i + 3 - k_i s_i - \gamma_i(f_i - 1) \quad (7)$$

$$\frac{df_i(t)}{dt} = s_i \quad (8)$$

$$\tau_i \frac{dv_i(t)}{dt} = f_i - v_i^{1/\alpha} \quad (9)$$

$$\tau_i \frac{dq_i(t)}{dt} = \frac{f_i\left(1 - (1 - p_i)^{1/f_i}\right)}{p_i} - \frac{q_i v_i^{1/\alpha}}{v_i} \quad (10)$$

Here, ρ denotes the resting oxygen extraction fraction, τ is a time constant and α represents the resistance of the veins. To compute in each area n, the BOLD signal, B_n, we calculate a volume-weighted sum of extra- and intravascular signals, which comprises a static nonlinear function of volume, v_n, and deoxyhaemoglobin content, q_n, and is expressed as follows:

$$B_n = V_0\left[\left(k_1(1 - q_n) + k_2\left(1 - q_n/v_n\right) + k_3(1 - v_n)\right)\right] \quad (11)$$

We used the original biophysical parameters (Stephan et al., 2007). To focus on the most functionally relevant frequency range in resting-state conditions, we applied a bandpass filter to both empirical and simulated BOLD signals ($0.08 > f > 0.008$ Hz) (Biswal et al., 1995; Glerean et al., 2012).

2.7. Generative effective connectivity calculation

Generative Effective Connectivity (GEC) is a general framework that, in an iterative process, utilizes differences detected at different times in the simulated signals between connected pairs of brain regions to infer the effective effect one brain region has on the other. The analysis of the GEC incorporates an indirect metric (as it is derived from other presented metrics) into the DMF whole-brain model to replace the existing descriptive metrics of FC and SC, providing a better fit to empirical data than with any previous method. Previous studies have shown how the GEC is a fundamental tool for understanding the propagation of information in structural networks (Gilson et al., 2016; Jobst et al., 2017). Methods for estimating GEC are explained in detail in a previous publication (Kringelbach et al., 2023). Here we provide a summary.

We computed the distance between the output of our model (i.e., the DMF) and the empirical grand average phase coherence matrices (as a measure of synchronization of the system) of the empirical BOLD signals from the healthy controls group. For the stroke patients' group, in an iterative procedure, we adjusted each structural connection separately (i.e., individually) using a greedy version of the gradient-descent approach. To work only with positive values for the algorithm, all values were transformed into a mutual information measure (assuming a Gaussian distribution). Also, the individual subject information is introduced by means of its disconnection mask, computing the group average SC in combination with each subject's SDC, derived from the Lesion Quantification Toolkit, as described above. The SC matrix was normalized to be comparable across subjects. We then fit the connectivity matrix C such that the model optimally reproduces the empirically measured covariances $FC^{empirical}$ (i.e., the normalized covariance matrix of the functional neuroimaging data) and the empirical time-shifted covariances $FS^{empirical}(\tau)$ where τ is the time lag. The $FC^{empirical}$ are normalized for each pair of regions j and k, using the shifted covariance matrix, by $\sqrt{KS_{jk}^{empirical}(0)KS_{jk}^{empirical}(0)}$. These computations are iteratively repeated for each C, update until the fit is fully optimized. At each step, the anatomical connectivity matrix C is updated (For more information, see (Deco et al., 2023)) as:

$$C_{jk} = C_{jk} + \varepsilon\left(FC_{jk}^{emp} - FC_{jk}^{mod}\right) + \varepsilon'\left(FS_{jk}^{emp}(\tau) - FS_{jk}^{mod}(\tau)\right). \quad (12)$$

As we can see, C is updated with the difference between the grand-averaged phase coherence matrices (Empirical: FC_{jk}^{emp} and model: FC_{jk}^{mod}) and the difference between the time-shifted covariance matrices, both scaled by factor $\varepsilon = 0.005$ and $\varepsilon' = 0.001$. Here, $FS_{jk}^{mod}(\tau)$ is defined similarly to $FS_{jk}^{emp}(\tau)$. After this process, C is considered as a GEC matrix. As we see, the prediction, therefore, is based on the current estimation of the structural connectivity, which gets updated optimizing the phase FC in each iteration. The model was run repeatedly with iterative updates of GEC until convergence was reached. The distinction between functional and effective connectivity is crucial here: FC is defined as the statistical dependence between the neurophysiological activity of brain regions, whereas GEC is defined as the influence one neural system exerts over another, thus providing directionality in the relations and making the matrices asymmetrical (Friston, 2011; Friston et al., 2003).

2.8. Models

- **"Non-Slow-wave Sleep (non-SWS)" Predictive model**

We calculated a predictive model to capture the dynamical effects of stroke lesions between one and two weeks after onset. First, we computed the GEC, as described before, on the same group. Next, for each stroke patient, we added the information of the individual SDC masks to the existing GEC to simulate fMRI BOLD data of the corresponding patient. As a result, the simulated time series (referred to as "Predictive model") contains structural information of the patient. It is important to remark that this procedure does not use the functional information of the patients, thus making it a predictive model, in contrast to the previously discussed non-predictive models (Idesis et al., 2024a).

- **"Slow-wave sleep (SWS)" model**

As reported in the previous section, the GEC of the healthy control group was calculated first, and then the SDC mask of each patient was added to the existing structural template to obtain the final SC for each stroke patient. The main difference with the previously described non-***SWS*** model is the addition of a sine wave as an intrinsic oscillation before transforming the simulated excitatory firing rate into the simulated BOLD signal in the nodes embedded in the perilesional area. This is done by adding an extra intrinsic sinus-shaped oscillation at the excitatory current in Eq. 1 for perilesional areas surrounding the lesion nodes. The size of the perilesional areas was set to 1 cm (Euclidean distance) around the lesioned areas, based on previous works (Russo et al., 2021; Sarasso et al., 2020). Extended perilesional sizes were also contemplated to probe their effect in the model (Fig. 2d). To find the optimal parameters for each subject, we performed an exploration of the possible oscillatory waves (Amplitudes: 0.01,0.05,0.1,0.25; Frequencies: 1, 2, 3, 4). We used as the optimal point for each patient the combination in which the difference with the ***non-SWS*** was highest.

- **Surrogate models**

To assess the validity of our results, we compared the performance of the ***SWS*** model with three different surrogate models. The first contained the correct lesion information but the parameters of the slow wave oscillations were randomly replaced from another subject. The second contained the correct addition of the delta oscillations but the lesion mask of a different subject. Lastly, the third contained both the lesion and the SW signal, from a different patient instead of the corresponding one. The performance comparison between the original model and the surrogate ones is observed in Fig. 3a.

3. Results

To infer the dynamical effects of stroke lesions two weeks after onset, we used an averaged structural matrix from the healthy control group (Fig. 1a**, left**) as input for a computational model based on biophysically grounded assumptions, referred as "Dynamic mean Field" model (Fig. 1a**, center**). The accuracy of the model in healthy controls is depicted in **Supp** Fig. 1. We used this model to compute as output, besides the simulated BOLD signal, the Generative Effective Connectivity (GEC), which captures directional interactions between regions by comparing at different times in the simulated signals the regions' connections (Fig. 1a**, right**). In the current study, we used only the functional data of the healthy control dataset ($n = 27$) to optimize the GEC parameters at the group level. By initializing the GEC to be equal to the

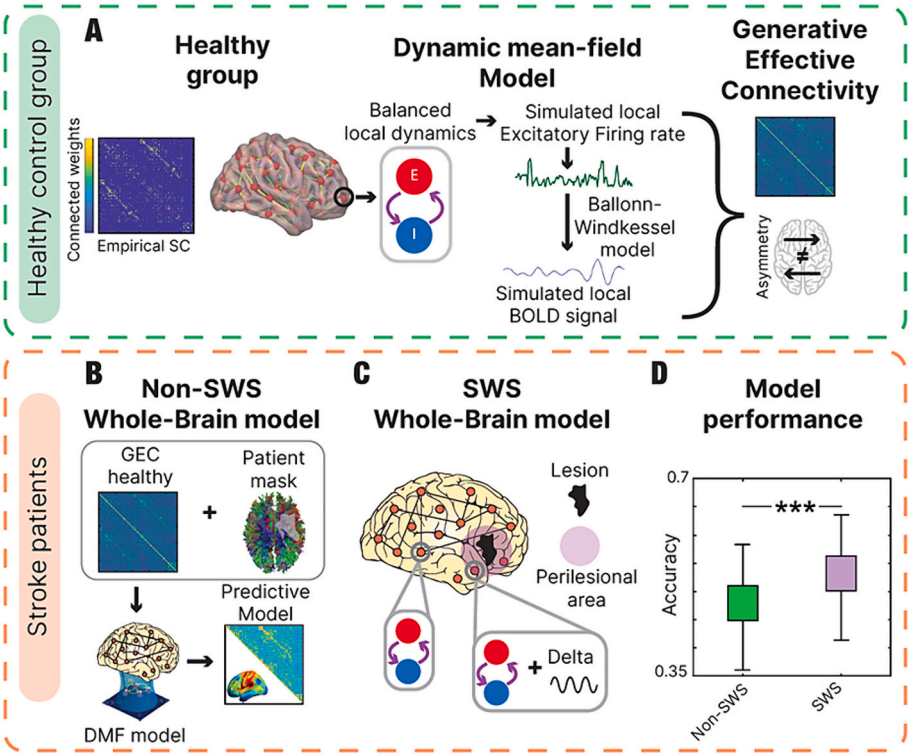

Fig. 1. Pipeline for the ***SWS*** whole-brain model: **(A)** Overview of the Generative Effective Connectivity (GEC) calculation: We considered 200 cortical regions from the Schaefer parcellation, and 34 subcortical and cerebellar regions from the AAL and Harvard-Oxford atlas. In the schematic brain, circles are brain regions and connections between brain regions are colored according to their connection weight. The local dynamics of each brain region are simulated by recurrently connected pools of excitatory (E, red circle) and inhibitory (I, blue circle) neuronal populations. In turn, brain regions are connected among themselves through the E pools, such that the excitatory inputs from other regions are weighted according to their respective connection weight. The connection from the I pool to the E one - Jn, the local inhibitory feedback - compensates for the excess of excitatory activity injected from other regions to keep each region's activity at a frequency of approximately 3 Hz. The simulated firing rate of each excitatory pool is used to generate BOLD-like signals for each brain region using the Balloon-Windkessel model. Healthy control GEC was calculated by using the healthy average SC as template with each healthy control fMRI time series. The model was optimized using the previously mentioned whole-brain model to create an average GEC for the healthy controls which provides asymmetrical structural information. **(B)** The ***non-SWS*** whole-brain predictive model uses each patient's disconnection mask to modify the control GEC and obtain the patient's simulated FC**. (C)** The ***SWS*** whole-brain model adds to the nodes within the perilesional region a delta oscillation in their corresponding simulated local excitatory firing rate, to replicate the after-stroke effects more accurately. **(D)** The model performance was compared between the ***non-SWS*** and ***SWS*** models to assess the influence of the addition of the slow wave oscillations in the model. The results show a significant enhancement of the model performance once the delta waves are added to the corresponding nodes ($p < .001$). (For interpretation of the references to colour in this figure legend, the reader is referred to the web version of this article.)

Structural Connectivity (SC), we iteratively adjusted its values to get an effective connectivity that maximizes the similarity between the model and empirical FC at a (healthy) group level.

We then superimposed the structural disconnection mask of each individual patient to the healthy group GEC to simulate the structural damage caused by stroke, creating a predictive model that generated a simulated version of each patient's FC matrix (Fig. 1b, **left**). Therefore, in contrast to most previously reported models, this predictive model simulates a patient's FC matrix using only the functional data of healthy control subjects; plus the structural disconnection (SDC) mask. We labelled this model as ***non-SWS*** whole-brain model, to differentiate it from the next model, where slow waves are included. This model was compared with two different surrogates (including a disconnection mask from a different patient or without any mask) to assess its validity (**Supp** Fig. 2). Finally, we developed the Slow-Wave Sleep (***SWS***) whole-brain model, where the nodes in the assumed peri-lesional area had a slow-wave oscillation incorporated in the nodal dynamics (Fig. 1c). The outcome of this last model allows us to assess the influence of the peri-lesional regional dynamics in the after-stroke effects. Model performance was assessed through Pearson's correlation between the (upper triangular part of) the simulated and experimental FC matrices. The comparison of the model performance with and without the inclusion of the slow-wave oscillations is depicted in Fig. 1d showing a significantly better performance of the ***SWS*** model ($t(95) = 17.86$, $p < .001$). An

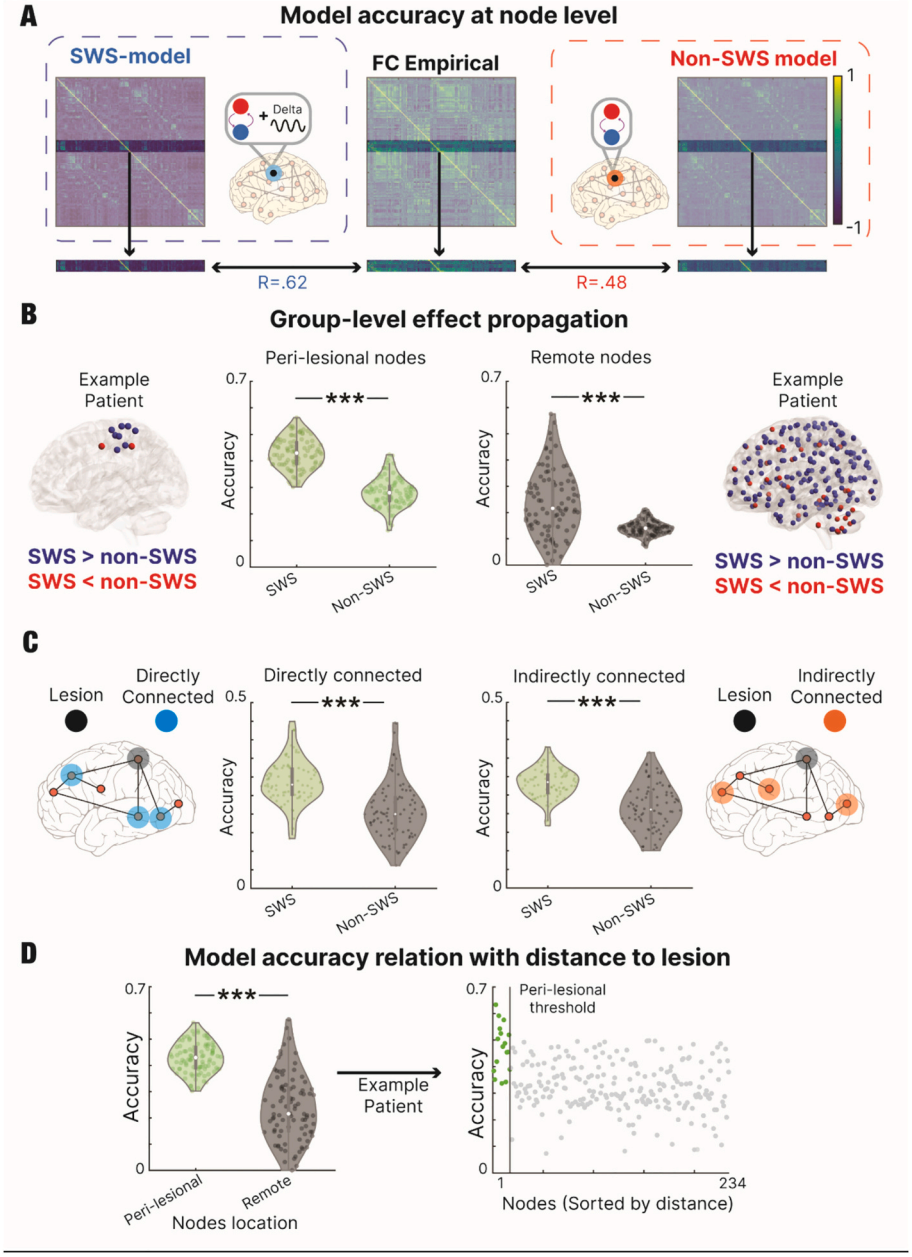

Fig. 2. SWS model accuracy and propagation effects: **(A)** Correlation between each empirical node and the corresponding simulation was assessed to explore which model shows a higher accuracy for that node (with or without slow-wave oscillation inclusion). **(B)** We inspected which nodes displayed a higher accuracy in the ***SWS*** model than in the ***non-SWS*** model (without added oscillations). Renders display at each ROI which model was more accurate. At a group level, the ***SWS*** showed a significantly higher accuracy in both peri-lesional (left render) and remote nodes (right render). **(C)** The accuracy of the remote nodes was disentangled between the nodes directly and indirectly connected to the peri-lesional nodes showing a significant increase in both cases when including the slow oscillations in the model **(D)** The relation between the accuracy of the model and the distance to the lesion was inspected showing significantly higher accuracy of the ***SWS*** model in the peri-lesional nodes. At the subject level, we found a negative trend where the highest accuracy corresponds to the nodes closer to the damaged area.

example of the dependency of the ***SWS*** model performance on the ***SWS*** parameters (Frequency and amplitude of the oscillation) is shown in **Supp** Fig. 3a. In the case of several positive alternatives, the combination of parameters with the highest difference was selected. Although the optimal parameters are patient-specific, most of the patients had their optimal values in the amplitude 0.01 and the frequencies 3 and 4 (**Supp** Fig. 3b). The influence of the oscillation phase in the model was assessed showing no significant impact (**Supp Fig. 5**).

3.1. Propagation effects

Next, we inspected if the addition of slow-wave oscillations affected only the manipulated nodes or if the effects could be observed throughout the brain. With that goal in mind, we compared the behavior of each empirical node with both models (***SWS*** and ***non-SWS***), testing whether the addition of slow oscillations increased or reduced the accuracy of the model for that specific region (Fig. 2a). We defined an accuracy for each node as the Pearson correlation between the node's simulated and empirical FC values (corresponding rows of the simulated and empirical FC matrix) and we compared the accuracy of the nodes corresponding for both peri-lesional and remote nodes. To achieve this goal, we inspected how many nodes were more accurately described by the ***SWS*** model in comparison to the ***non-SWS*** model (Fig. 2b**,** left and right extremes). The comparison showed that the ***SWS*** model has a higher performance both in the peri-lesional nodes ($(t(89) = 20.69$, $p < .001$), Fig. 2b, center-left) and, quite remarkably, in the remote nodes ($(t(89) = 49.44$, $p < .001$), Fig. 2b, center-right).

In addition, we compared the performance in the model by assessing the accuracy of the directly connected and indirectly connected nodes to the perilesional region. The comparison showed a significant difference between the ***SWS*** and ***non-SWS*** model in both directly connected ($(t(87) = 14.5$, $p < .001$), and indirectly connected nodes ($(t(87) = 15.45$, $p < .001$) (Fig. 2c).

Lastly, we calculated the relation between the model accuracy and the distance of the nodes to the lesion (Fig. 2d). We found a significantly improved performance of the ***SWS*** model in the peri-lesional nodes compared to the remote nodes ($t(89) = 12.53$, $p < .001$). Furthermore, at the subject level, there was a negative relation between the variables, where the nodes closer to the damaged area showed a higher accuracy.

In summary, the addition of slow-wave oscillations to the model caused a clear effect in the simulated brain activity, spreading across many regions including those distant from the lesion. Furthermore, the relation of accuracy with the distance from the lesion allows the comparison of these results with previously reported ones (Russo et al., 2021; Sarasso et al., 2020). The presented model, based on this, can replicate the after-stroke effects not only in the peri-lesional region (where the manipulation was performed) but, more importantly, throughout the whole brain.

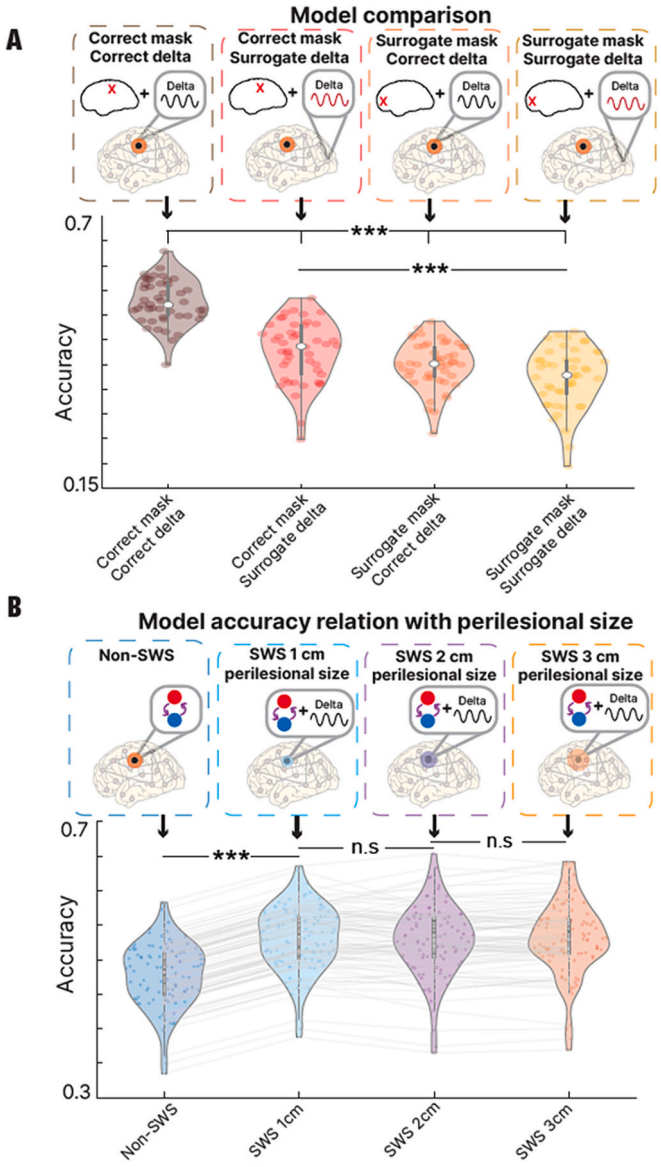

Fig. 3. Model validity among conditions and model accuracy dependency on the perilesional area size: **(A)** Accuracy of the models when using the subject mask and stimulated nodes correctly or shuffled. The highest accuracy was observed when the lesion and the manipulated nodes were correctly corresponding to the subject. **(B)** We assessed the influence of the perilesional size by running the model with different diameters for this region (1, 2 and 3 cm). By comparing the different parameters, we observed a significant difference between the ***non-SWS*** and the ***SWS*** model ($p < .001$) while no significant difference between the distinct peri-lesional sizes.

3.2. Model validity

We aimed to assess the influence of each feature on the model by modifying the two principal inputs (lesion mask and slow-wave oscillations). With this goal, we compared the validity of the ***SWS*** against null models where the mask and the added slow waves were manipulated (Fig. 3a). We found a significant difference in accuracy between the models ($F(3,180) = 7.35$, $p < .001$) where the original ***SWS*** showed the highest accuracy (significantly higher than the other three models, $p < .001$), followed by the model with correct mask, the model with the correct delta oscillations and finally the model with both parameters shuffled. There was also observed a significant difference between the second model (correct mask and surrogate delta) and the fourth model (surrogate mask and surrogate delta) ($p < .001$), while there was no significance in the remaining comparisons.

Lastly, we tested the influence of the distance criterion used to define the perilesional area affected by SWS in the model (1, 2 and 3 cm). We observed a significant difference between the ***non-SWS*** and the ***SWS*** model ($p < .001$) while no significant difference between the distinct peri-lesional sizes ($p > .9$) (Fig. 3b), showing that the original assumption of a 1 cm padding suffices to characterize the perilesional area. An extended version is displayed in **Supp. Fig. 4** where the last model is compared to a model where both the surrogate mask and the surrogate slow oscillations are obtained from the same patient, showing similar results. Also, the lack of significant differences between the three size shows the strong influence of the slow-wave oscillations of the perilesioned nodes on their surroundings.

In summary, we observed that the accuracy of the model critically depends on including the specific patient's disconnection mask (not just a generic disconnection) and adding slow-save oscillations in the perilesional area (and not just a random area), while the performance

enhancement due to the addition of slow-wave oscillations in the perilesional nodes can be achieved with a relatively strict definition of the perilesional area (1 cm from the lesion).

4. Discussion

In this study, we compared measured the effect of a putative neurophysiological marker of disconnection, i.e., delta wave activity near the lesion, on the accuracy of different whole-brain models in predicting the FC patterns of stroke patients. Both the pattern of structural disconnection inferred from a healthy atlas of white matter connections and the presence of perilesional delta wave activity improved the fit of the functional connectivity of the model with the empirically functional connectivity in the same patients. This result shows for the first time in-silico that perilesional delta wave activity contributes to the abnormal functional connectivity caused by focal stroke lesions, not only near the lesion, but also at a distance in connected regions.

We first fitted the model to data from age- and education-matched healthy controls based on a healthy structural connectome and the healthy controls subjects functional imaging data. Then, we modified the healthy model to make it specific to the patient. As in previous literature (Griffis et al., 2019; Idesis et al., 2022b), we obtained a disconnection mask by overlapping the patient's segmented lesion with a streamline tractography atlas, determining the proportion of streamlines between each pair of regions that are interrupted by the lesion. This atlas-based procedure does not require patient-specific tracking of structural connections, but only the segmentation of the lesion that can be obtained through clinical scans. It could be validated with direct measures of SC disconnection based on diffusion imaging. For each patient, we then determined how the patient's lesion modified the healthy structural connectome and made corresponding changes to the structural connectivity parameters in the healthy model (the GEC parameters) without additional model fitting and without using the patient's functional data. We thus, generated patient-specific predicted FC, which was compared against the empirically measured FC. Specifically, model accuracy was evaluated by assessing the correlation between the patient's empirical and predicted FC matrices. Because FC matrices specify the functional interactions between each pair of brain regions, the predicted matrices potentially provide information concerning which functional connections are particularly affected by lesions in the patient (***non-SWS*** model). Lastly, by incorporating slow-wave oscillations in the peri-lesional nodes, we managed to enhance the efficiency of the model to create a more accurate representation of the lesion consequences (***SWS*** model).

The findings indicate that a comprehensive brain computational model can accurately predict functional connectivity in patients solely based on the structural disconnections resulting from their brain lesions and the group-level healthy connectome. This suggests that this biophysical model, to some extent, mechanistically captures the link between anatomical structure and functional activity. Additionally, incorporating slow-wave oscillations in nodes near the lesion improved the model's performance in predicting the observed fMRI connectivity. This agrees with recent literature finding SWS activity in the perilesional area (Russo et al., 2021; Sarasso et al., 2020). This research strongly suggests that slow-wave activity arising in the perilesional area influences distal areas, with an effect on functional interactions (connectivity) onto regions connected to the lesion.

There are two possible explanations for these remote effects of delta waves. First, distal areas are disconnected anatomically from/to the lesion either through callosal connections or long-range intrahemispheric connections. Another possible intra-hemispheric disconnection can involve subcortical regions of the thalamus or basal ganglia. This disconnection can lead to the generation in remote areas of local slow wave activity. As discussed previously (Sanchez-Vives et al., 2017; Sarasso et al., 2020) slow wave activity emerges spontaneously when tissue is disconnected from other inputs suggesting that slow waves represent a "default' functional state of cortex controlled by intrinsic mechanisms of excitability (up/down states).

Second, abnormal delta wave activity can propagate to distant sites through a dynamic phenomenon of attraction. Specifically, a strong source of activity (oscillatory or not) in the perilesional cortex can cause "dynamic" attraction of connected regions. This result is supported by the gradual modulation of slow waves going from perilesional to directly vs. indirectly disconnected regions. Indirectly disconnected regions, two or more synapses away from the lesion, plausibly would show a modulation mainly through dynamic attraction.

These findings and the effects of slow-waves on resting state functional networks shall be tested empirically by measuring both fMRI and EEG connectivity in the same stroke patients.

Furthermore, this study offers a fresh perspective on the dynamical consequences of brain injuries. Drawing inspiration from previous research demonstrating EEG slowing in perilesional areas (Butz et al., 2004; Russo et al., 2021; Sarasso et al., 2020), we establish a direct connection between the electrophysiological patterns seen in local sleep, extensively documented in the sleep literature, and the pathophysiology of focal brain injuries and strokes (Sarasso et al., 2020). Literature is rich in reports on how stroke affects the power of different EEG frequency bands (Finnigan et al., 2016; Finnigan and van Putten, 2013). Recent findings (Sarasso et al., 2020), using TMS-EEG, showed clear differences in TMS-evoked oscillatory activity between cortical and non-cortical lesions. Regarding the lesion localization, previous literature reports clear spectral changes in middle cerebral artery cortical strokes (Fanciullacci et al., 2017), while similar evidence is less consistent for subcortical, lacunar and posterior circulation strokes (Macdonell, 1988).

By connecting the notion of local sleep to the pathophysiology of focal brain injury and stroke, perilesional off-periods may represent a valid clinical indicator of the state of discrete cortical circuits following brain injury as well as a potential target for the development of novel therapeutic interventions and physical rehabilitation aimed at fostering functional recovery (Sarasso et al., 2020). Various factors may explain this perilesional effect as explained extensively in a recent review from Massimini and colleagues (Massimini et al., 2024). First, local edema, as observed in animal models (Russo et al., 2021). Second, the expression of slow waves in the perilesional regions may reflect lack of input from ascending activating systems due to damage of white matter fibers (Russo et al., 2021). The disconnection of cortical regions often results in the expression of slow waves as a default activity pattern of the cortical circuits (Sanchez-Vives, 2015; Sanchez-Vives et al., 2017). One interesting possibility is that slow waves might be protective and beneficial in the acute recovery phase (decreasing the energy consumption near the damage region) and then become detrimental if they persist indefinitely into the chronic phase. While the current study explains the local and long-range effects of this phenomenon on functional connectivity, the origin of this slow-wave dynamic is out of the current scope.

In this context, the presence of lesions involving both white and gray matter in patients seems to be particularly suited in producing EEG slow waves and off-periods in response to a direct cortical perturbation. Although the precise assessment of the effects of lesion size and location is beyond the scope of the present work, the inclusion of a larger sample of patients affected by cortico-subcortical lesion with different volumes and locations (Tscherpel et al., 2020) represents an interesting venue for future studies. At the same time, performing multiple, controlled stimulations while systematically increasing the distance with respect to the lesion boundaries will also allow assessing the precise spatial extent of perilesional areas (Sarasso et al., 2020), allowing us to better constrain the ***SWS*** model. Furthermore, it would be relevant to develop predictive whole-brain computer models of individual patients with stroke to simulate different personalized stimulation protocols with the goal of normalizing abnormal local and global dynamics (Perl et al., 2023). In particular, one could test whether the suppression or enhancement of slow waves, achieved by means of appropriate stimulation, would shift the patient's resting state dynamics closer or farther from normal activity, and use this information to assist recovery treatment.

In conclusion, the information obtained from these models could be used for optimizing treatment protocols combining stimulation with behavioral training, adding the potential to influence the progression of stroke rehabilitation by modulating slow waves during specific time intervals.

4.1. Limitations

The primary objective of this study was to shed light on the connection between sleep-like slow oscillations in perilesional areas and the consequences of strokes. However, it remains unclear how the slow oscillations change as patients recover. Subsequent research endeavors could leverage this longitudinal dataset to explore and answer these specific questions. Additionally, it's worth noting that the dataset predominantly comprises ischemic stroke patients, and it would be prudent to replicate these findings in hemorrhagic stroke cases before extending the conclusions to encompass all stroke patients.

At this point it is important to mention that the original studies by Russo and coworkers (Russo et al., 2021) used a different imaging technology (sEEG) than the one we use here (fMRI), observing important sleep-like activity in frequencies below 4 Hz. Although fMRI is far from linear in its responses to neural activity (Robinson et al., 2006), the frequencies reported in this work (1–4 Hz) also present important discrepancies in perilesional activity with respect to healthy areas, thus rendering valid the current analysis. Furthermore, the presented hemodynamic model (BW) is merely one approach to link the oscillatory signal to fMRI data. Further studies containing longer electrophysiological data (Idesis et al., 2024b), or even both modality formats could explore the robustness of the model.

5. Conclusion

In conclusion, the addition of slow-wave oscillations in the perilesional region enhanced the accuracy of the model replicating with higher precision the consequences of stroke on functional connectivity, both in the affected area and in distant areas at the whole-brain level. This model can provide unique insights into how strokes disrupt resting brain organization and the propagation of the corresponding effects across the brain, opening many venues for treatment and more efficient recoveries. Through generative whole-brain models, linking the engagement of cortical sleep-like dynamics to focal brain injury provides a plausible biophysical mechanistic explanation for diaschisis effects in the resting state connectivity of stroke patients. Furthermore, the availability of a computational model, allowing for controlled analysis of the local and distal effects of SWS, may open new clinical possibilities, such as positively affecting stroke rehabilitation by dampening or enhancing slow waves in specific time windows.

Funding

S·I is supported by the project NEurological MEchanismS of Injury, and Sleep-like cellular dynamics (NEMESIS) (ref. 101071900) funded by the EU ERC Synergy Horizon Europe. G.P. is supported by Grant PID2021-122136OB-C22 funded by MCIN/AEI/ 10.13039/501100011033 and by ERDF A way of making Europe. G.D. is supported by 10.13039/50110001103310.13039/501100011033Grant PID2022-136216NB-I00 funded by MICIU/AEI/10.13039/501100011033 and by "ERDF A way of making Europe", "ERDF, EU". MVSV is supported by PID2020-112947RB-I00 AEI /10.13039/501100011033, funded by the Spanish Ministry of Science, Innovation and Universities (MCIU). MC is supported by Fondazione Cassa di Risparmio di Padova e Rovigo (CARIPARO)(GA number 55403); Ministry of Health Italy: NEUROCONN (RF-2008 -12366899); H2020 European School of Network Neuroscience- euSNN, H2020-SC5–2019-2, (Grant Agreement number 869505); Ministry of Health Italy: EYEMOVINSTROKE (RF-2019-12369300);

CRediT authorship contribution statement

Sebastian Idesis: Visualization, Methodology, Formal analysis, Conceptualization, Writing – review & editing, Writing – original draft. **Michele Allegra:** Methodology, Formal analysis, Writing – review & editing. **Jakub Vohryzek:** Visualization, Methodology, Writing – review & editing. **Yonatan Sanz Perl:** Methodology, Formal analysis, Writing – review & editing. **Maria V. Sanchez-Vives:** Writing – review & editing. **Marcello Massimini:** Writing – review & editing. **Maurizio Corbetta:** Conceptualization, Writing – review & editing. **Gustavo Deco:** Conceptualization, Writing – review & editing, Writing – original draft.

Declaration of competing interest

Marcello Massimini is co-founder of Intrinsic Powers, a spin-off of the University of Milan.

Data availability

Data will be made available on request.

Acknowledgments

We thank Melina Timplalexi for assisting with the figures.

Appendix A. Supplementary data

Supplementary data to this article can be found online at https://doi.org/10.1016/j.nbd.2024.106613.

References

Andrillon, T., Burns, A., Mackay, T., Windt, J., Tsuchiya, N., 2021. Predicting lapses of attention with sleep-like slow waves. Nat. Commun. 12 https://doi.org/10.1038/s41467-021-23890-7, 3657–3657.

Biswal, B., Zerrin Yetkin, F., Haughton, V.M., Hyde, J.S., 1995. Functional connectivity in the motor cortex of resting human brain using echo-planar mri. Magn. Reson. Med. 34, 537–541. https://doi.org/10.1002/mrm.1910340409.

Brott, T., Adams, H.P., Olinger, C.P., Marler, J.R., Barsan, W.G., Biller, J., Spilker, J., Holleran, R., Eberle, R., Hertzberg, V., 1989. Measurements of acute cerebral infarction: a clinical examination scale. Stroke 20, 864–870. https://doi.org/10.1161/01.str.20.7.864.

Butz, M., Gross, J., Timmermann, L., Moll, M., Freund, H.-J., Witte, O.W., Schnitzler, A., 2004. Perilesional pathological oscillatory activity in the magnetoencephalogram of patients with cortical brain lesions. Neurosci. Lett. 355, 93–96. https://doi.org/10.1016/j.neulet.2003.10.065.

Camassa, A., Galluzzi, A., Mattia, M., Sanchez-Vives, M.V., 2022. Deterministic and stochastic components of cortical down states: dynamics and modulation. J. Neurosci. 42, 9387–9400. https://doi.org/10.1523/JNEUROSCI.0914-22.2022.

Carrera, E., Tononi, G., 2014. Diaschisis: past, present, future. Brain 137, 2408–2422. https://doi.org/10.1093/brain/awu101.

Clarkson, A.N., Huang, B.S., Macisaac, S.E., Mody, I., Carmichael, S.T., 2010. Reducing excessive GABA-mediated tonic inhibition promotes functional recovery after stroke. Nature 468, 305–309. https://doi.org/10.1038/nature09511.

Corbetta, M., Ramsey, L., Callejas, A., Baldassarre, A., Hacker, C.D., Siegel, J.S., Astafiev, S.V., Rengachary, J., Zinn, K., Lang, C.E., Connor, L.T., Fucetola, R., Strube, M., Carter, A.R., Shulman, G.L., 2015. Common behavioral clusters and subcortical anatomy in stroke. Neuron 85, 927–941. https://doi.org/10.1016/j.neuron.2015.02.027.

Deco, G., Jirsa, V.K., 2012. Ongoing cortical activity at rest: criticality, multistability, and ghost attractors. J. Neurosci. 32, 3366–3375. https://doi.org/10.1523/JNEUROSCI.2523-11.2012.

Deco, G., Jirsa, V., McIntosh, A.R., Sporns, O., Kötter, R., 2009. Key role of coupling, delay, and noise in resting brain fluctuations. Proc. Natl. Acad. Sci. USA 106, 10302–10307. https://doi.org/10.1073/pnas.0901831106.

Deco, G., Hagmann, P., Hudetz, A.G., Tononi, G., 2014a. Modeling resting-state functional networks when the cortex falls asleep: local and global changes. Cereb. Cortex 24, 3180–3194. https://doi.org/10.1093/cercor/bht176.

Deco, G., Ponce-Alvarez, A., Hagmann, P., Romani, G.L., Mantini, D., Corbetta, M., 2014b. How local excitation-inhibition ratio impacts the whole brain dynamics. J. Neurosci. 34, 7886–7898. https://doi.org/10.1523/JNEUROSCI.5068-13.2014.

Deco, G., Lynn, C.W., Sanz Perl, Y., Kringelbach, M.L., 2023. Violations of the fluctuation-dissipation theorem reveal distinct nonequilibrium dynamics of brain states. Phys. Rev. E 108. https://doi.org/10.1103/physreve.108.064410.

Die Lokalisation im Grosshirn und der Abbau der Funktion durch Kortikale Herde, 1914. J. Am. Med. Assoc. LXIII 797. https://doi.org/10.1001/jama.1914.02570090083033.

Falcon, M.I., Riley, J.D., Jirsa, V., McIntosh, A.R., Chen, E.E., Solodkin, A., 2016. Functional mechanisms of recovery after chronic stroke: modeling with the virtual. Brain eNeuro 3. https://doi.org/10.1523/ENEURO.0158-15.2016. ENEURO.0158-15.2016.

Fanciullacci, C., Bertolucci, F., Lamola, G., Panarese, A., Artoni, F., Micera, S., Rossi, B., Chisari, C., 2017. Delta power is higher and more symmetrical in ischemic stroke patients with cortical involvement. Front. Hum. Neurosci. 11 https://doi.org/10.3389/fnhum.2017.00385, 385–385.

Finnigan, S., van Putten, M.J.A.M., 2013. EEG in ischaemic stroke: quantitative EEG can uniquely inform (sub-)acute prognoses and clinical management. Clin. Neurophysiol. 124, 10–19. https://doi.org/10.1016/j.clinph.2012.07.003.

Finnigan, S., Wong, A., Read, S., 2016. Defining abnormal slow EEG activity in acute ischaemic stroke: Delta/alpha ratio as an optimal QEEG index. Clin. Neurophysiol. 127, 1452–1459. https://doi.org/10.1016/j.clinph.2015.07.014.

Friston, K.J., 2011. Functional and effective connectivity: a review. Brain Connect. 1, 13–36. https://doi.org/10.1089/brain.2011.0008.

Friston, K.J., Harrison, L., Penny, W., 2003. Dynamic causal modelling. NeuroImage 19, 1273–1302. https://doi.org/10.1016/s1053-8119(03)00202-7.

Gilson, M., Moreno-Bote, R., Ponce-Alvarez, A., Ritter, P., Deco, G., 2016. Estimation of directed effective connectivity from fMRI functional connectivity hints at asymmetries of cortical connectome. PLoS Comput. Biol. 12 https://doi.org/10.1371/journal.pcbi.1004762 e1004762–e1004762.

Glerean, E., Salmi, J., Lahnakoski, J.M., Jääskeläinen, I.P., Sams, M., 2012. Functional magnetic resonance imaging phase synchronization as a measure of dynamic functional connectivity. Brain Connect. 2, 91–101. https://doi.org/10.1089/brain.2011.0068.

Griffis, J.C., Metcalf, N.V., Corbetta, M., Shulman, G.L., 2019. Structural disconnections explain brain network dysfunction after stroke. Cell Rep. 28 https://doi.org/10.1016/j.celrep.2019.07.100, 2527–2540.e9.

Griffis, J.C., Metcalf, N.V., Corbetta, M., Shulman, G.L., 2021. Lesion quantification toolkit: a MATLAB software tool for estimating grey matter damage and white matter disconnections in patients with focal brain lesions. Neuroimage Clin. 30 https://doi.org/10.1016/j.nicl.2021.102639, 102639–102639.

Herzog, R., Mediano, P.A.M., Rosas, F.E., Luppi, A.I., Perl, Y.S., Tagliazucchi, E., Kringelbach, M., Cofré, R., Deco, G., 2022. Neural Mass Modelling for the Masses: Democratising Access to Whole-Brain Biophysical Modelling with FastDMF. https://doi.org/10.1101/2022.04.11.487903.

Idesis, S., Faskowitz, J., Betzel, R.F., Corbetta, M., Sporns, O., Deco, G., 2022a. Edge-centric analysis of stroke patients: an alternative approach for biomarkers of lesion recovery. Neuroimage Clin. 35 https://doi.org/10.1016/j.nicl.2022.103055, 103055–103055.

Idesis, S., Favaretto, C., Metcalf, N.V., Griffis, J.C., Shulman, G.L., Corbetta, M., Deco, G., 2022b. Inferring the dynamical effects of stroke lesions through whole-brain modeling. Neuroimage Clin. 36 https://doi.org/10.1016/j.nicl.2022.103233, 103233–103233.

Idesis, S., Allegra, M., Vohryzek, J., Sanz Perl, Y., Faskowitz, J., Sporns, O., Corbetta, M., Deco, G., 2023. A low dimensional embedding of brain dynamics enhances diagnostic accuracy and behavioral prediction in stroke. Sci. Rep. 13 https://doi.org/10.1038/s41598-023-42533-z, 15698–15698.

Idesis, S., Allegra, M., Vohryzek, J., Yonatan, S.P., Metcalf, N.V., Griffis, J.C., Corbetta, M., Shulman, G.L., Deco, G., 2024a. Generative Whole-Brain Dynamics Models from Healthy Subjects Predict Functional Alterations in Stroke at the Level of Individual Patients. https://doi.org/10.1101/2024.01.02.573878.

Idesis, S., Geli, S., Faskowitz, J., Vohryzek, J., Sanz Perl, Y., Pieper, F., Galindo-Leon, E., Engel, A.K., Deco, G., 2024b. Functional hierarchies in brain dynamics characterized by signal reversibility in ferret cortex. PLoS Comput. Biol. 20 https://doi.org/10.1371/journal.pcbi.1011818 e1011818–e1011818.

Jobst, B.M., Hindriks, R., Laufs, H., Tagliazucchi, E., Hahn, G., Ponce-Alvarez, A., Stevner, A.B.A., Kringelbach, M.L., Deco, G., 2017. Increased stability and breakdown of brain effective connectivity during slow-wave sleep: mechanistic insights from whole-brain computational modelling. Sci. Rep. 7 https://doi.org/10.1038/s41598-017-04522-x, 4634–4634.

Kringelbach, M.L., Perl, Y.S., Tagliazucchi, E., Deco, G., 2023. Toward naturalistic neuroscience: mechanisms underlying the flattening of brain hierarchy in movie-watching compared to rest and task. Sci. Adv. 9 https://doi.org/10.1126/sciadv.ade6049 eade6049–eade6049.

Macdonell, R.A.L., 1988. The electroencephalogram and acute ischemic stroke. Arch. Neurol. 45, 520. https://doi.org/10.1001/archneur.1988.00520290048013.

Massimini, M., Corbetta, M., Sanchez-Vives, M.V., Andrillon, T., Deco, G., Rosanova, M., Sarasso, S., 2024. Sleep-like cortical dynamics during wakefulness and their network effects following brain injury. Nat. Commun. 15, 7207. https://doi.org/10.1038/s41467-024-51586-1.

Nita, D.A., Cisse, Y., Timofeev, I., Steriade, M., 2006. Waking-sleep modulation of paroxysmal activities induced by partial cortical Deafferentation. Cereb. Cortex 17, 272–283. https://doi.org/10.1093/cercor/bhj145.

Nuwer, M.R., Jordan, S.E., Ahn, S.S., 1987. Evaluation of stroke using EEG frequency analysis and topographic mapping. Neurology 37. https://doi.org/10.1212/wnl.37.7.1153, 1153–1153.

Perl, Y.S., Geli, S., Pérez-Ordoyo, E., Zonca, L., Idesis, S., Vohryzek, J., Jirsa, V.K., Kringelbach, M.L., Tagliazucchi, E., Deco, G., 2023. Whole-Brain Modelling of Low-Dimensional Manifold Modes Reveals Organising Principle of Brain Dynamics. https://doi.org/10.1101/2023.11.20.567824.

Poudel, G.R., Hawes, S., Innes, C.R.H., Parsons, N., Drummond, S.P.A., Caeyensberghs, K., Jones, R.D., 2021. RoWDI: rolling window detection of sleep intrusions in the awake brain using fMRI. J. Neural Eng. 18, 056063 https://doi.org/10.1088/1741-2552/ac2bb9.

Robinson, P.A., Drysdale, P.M., Van der Merwe, H., Kyriakou, E., Rigozzi, M.K., Germanoska, B., Rennie, C.J., 2006. BOLD responses to stimuli: dependence on frequency, stimulus form, amplitude, and repetition rate. NeuroImage 31, 585–599. https://doi.org/10.1016/j.neuroimage.2005.12.026.

Russo, S., Pigorini, A., Mikulan, E., Sarasso, S., Rubino, A., Zauli, F.M., Parmigiani, S., d'Orio, P., Cattani, A., Francione, S., Tassi, L., Bassetti, C.L.A., Lo Russo, G., Nobili, L., Sartori, I., Massimini, M., 2021. Focal lesions induce large-scale percolation of sleep-like intracerebral activity in awake humans. NeuroImage 234, 117964. https://doi.org/10.1016/j.neuroimage.2021.117964.

Sanchez-Vives, M.V., 2015. Slow wave activity as the default mode of the cerebral cortex. Arch. Ital. Biol. https://doi.org/10.12871/000398292014239.

Sanchez-Vives, M.V., Massimini, M., Mattia, M., 2017. Shaping the default activity pattern of the cortical network. Neuron 94, 993–1001. https://doi.org/10.1016/j.neuron.2017.05.015.

Sarasso, S., D'Ambrosio, S., Fecchio, M., Casarotto, S., Viganò, A., Landi, C., Mattavelli, G., Gosseries, O., Quarenghi, M., Laureys, S., Devalle, G., Rosanova, M., Massimini, M., 2020. Local sleep-like cortical reactivity in the awake brain after focal injury. Brain 143, 3672–3684. https://doi.org/10.1093/brain/awaa338.

Schaefer, A., Kong, R., Gordon, E.M., Laumann, T.O., Zuo, X.-N., Holmes, A.J., Eickhoff, S.B., Yeo, B.T.T., 2018. Local-global Parcellation of the human cerebral cortex from intrinsic functional connectivity MRI. Cereb. Cortex 28, 3095–3114. https://doi.org/10.1093/cercor/bhx179.

Siegel, J.S., Ramsey, L.E., Snyder, A.Z., Metcalf, N.V., Chacko, R.V., Weinberger, K., Baldassarre, A., Hacker, C.D., Shulman, G.L., Corbetta, M., 2016. Disruptions of network connectivity predict impairment in multiple behavioral domains after stroke. Proc. Natl. Acad. Sci. USA 113, E4367–E4376. https://doi.org/10.1073/pnas.1521083113.

Siegel, J.S., Seitzman, B.A., Ramsey, L.E., Ortega, M., Gordon, E.M., Dosenbach, N.U.F., Petersen, S.E., Shulman, G.L., Corbetta, M., 2018. Re-emergence of modular brain networks in stroke recovery. Cortex 101, 44–59. https://doi.org/10.1016/j.cortex.2017.12.019.

Stephan, K.E., Weiskopf, N., Drysdale, P.M., Robinson, P.A., Friston, K.J., 2007. Comparing hemodynamic models with DCM. Neuroimage 38, 387–401. https://doi.org/10.1016/j.neuroimage.2007.07.040.

Talozzi, L., Forkel, S.J., Pacella, V., Nozais, V., Allart, E., Piscicelli, C., Pérennou, D., Tranel, D., Boes, A., Corbetta, M., Nachev, P., Thiebaut de Schotten, M., 2023. Latent disconnectome prediction of long-term cognitive-behavioural symptoms in stroke. Brain 146, 1963–1978. https://doi.org/10.1093/brain/awad013.

Tscherpel, C., Dern, S., Hensel, L., Ziemann, U., Fink, G.R., Grefkes, C., 2020. Brain responsivity provides an individual readout for motor recovery after stroke. Brain 143, 1873–1888. https://doi.org/10.1093/brain/awaa127.

Tzourio-Mazoyer, N., Landeau, B., Papathanassiou, D., Crivello, F., Etard, O., Delcroix, N., Mazoyer, B., Joliot, M., 2002. Automated anatomical labeling of activations in SPM using a macroscopic anatomical Parcellation of the MNI MRI single-subject brain. NeuroImage 15, 273–289. https://doi.org/10.1006/nimg.2001.0978.